NRC Publications Archive
Archives des publications du CNRC

Common Path swept-source OCT interferometer with artifact removal

Vergnole, Sébastien; Lamouche, Guy; Dufour, Marc; Gauthier, Bruno

National Research Council Canada   Conseil national de recherches Canada

Canada

Common Path swept-source OCT interferometer with artifact removal

Sébastien VERGNOLE, Guy LAMOUCHE, Marc L. DUFOUR and Bruno GAUTHIER

IMI-NRC, 75 bd de Mortagne, Boucherville (Qc), J4B 6Y4, Canada

ABSTRACT

We present here the implementation of a fiber-based common-path interferometer for Swept Source Optical Coherence Tomography (SS-OCT). A common path configuration is often a suitable approach for increasing the stability of the measurements. Optical fibers are sensitive to temperature and some other mechanical perturbations which compromise absolute accuracy measurements. A common-path configuration provides a mean to define a reference at the probe location and, thereby, to compensate for the optical path length perturbations. Additionally, in SS-OCT, we have to deal with autocorrelation noise and the mirror image artifact due to the computation of the Fourier transform. Thus, our common-path implementation also includes acousto-optics modulators to remove the depth degeneracy as it has already been done when using a "traditional" interferometer configuration. The efficiency of our system is validated by comparing images acquired with a "traditional" SS-OCT configuration and with our common path SS-OCT configuration.

Keywords: Optical Coherence Tomography, Swept-Source OCT, Common-Path, Depth Ambiguity

1. INTRODUCTION

Optical fibers are sensitive to temperature and some other mechanical perturbations which might compromise absolute accuracy measurements. However, a common-path configuration provides a mean to define a reference at the probe location and, thereby, to compensate for the optical fiber path perturbations. The probe can be installed hundreds of meters away from the control unit while allowing micron range absolute accuracy. To our knowledge, the principles of common path interferometry as a tool for industrial inspection (film thickness gauge) was first disclosed in a patent from Flournoy in 1967.[1] He published a journal article about that in 1972.[2] In 1984, Bosselman et al.[3] proposed a common path configuration that was partly fibered. They also proposed a second interferometer to get accurate displacement measurement of the reference mirror. In 1995, Sorin et al.[4] obtained a patent for measuring film thickness by submitting a configuration very similar to the one proposed by Flournoy. The main differences reside in the extensive use of fiber-optic components and an adjustable focus for the probe. Common-path techniques have also been used for nearly one decade in our institute[5] mainly for industrial applications. These experiments were all carried out with time domain configurations.

In Fourier-domain optical coherence tomography (FD-OCT), some common-path setups have already been reported.[6–8] A patent application has also been published.[9] These configurations do not take into account the limitation inherent to any kind of FD-OCT setups: the mirror artifact due to the computation of the Fourier transform. Recently, a full range complex common-path spectral-domain OCT (SD-OCT) setup has been demonstrated.[10] Here, we present a common-path configuration in the specific case of swept-source OCT (SS-OCT) with artifact removal. Many techniques exist to remove the depth degeneracy using electro-optic modulator,[11] acousto-optic modulators[12,13] or 3x3 coupler.[14] Phase shifting[15] or transverse modulation methods are also used.[16–21]

In our work, acousto-optic modulators were used. We propose to measure some system's characteristics like the envelope stability and the sensitivity. Some images were acquired using different configurations to assess the artifact removal efficiency.

Further author information: (Send correspondence to S.V.)

S.V.: E-mail: Sebastien.Vergnole@cnrc-nrc.gc.ca, Telephone: 1 450 641 5137

2. EXPERIMENTAL SETUP

A common path configuration, similar to the one implemented in our laboratory, is illustrated in Fig. 1. The optical power from a Santec HSL-2000 swept-source with a 1320 nm center wavelength and a 117 nm scanning range is entirely fed to the sensing probe through an optical circulator. The probe fiber tip is cut to produce a first reflection that will be later used to interfere with the light reflected from the sample surface. The light is focused on the sample surface. The small reflected fraction is collected by the same lens and fed back in the same fiber in the reversed direction. Circulator 0 directs the two reflected light component (from the fiber tip and from the sample surface) to a Mach-Zehnder fiber-based reference interferometer. The two components from circulator 0 are split thanks to the 50:50 input coupler (Cp1). Half of the power is then transmitted into the two arms of the reference interferometer. This reference interferometer is fitted with acousto-optic modulators which provide a frequency shift of 10 MHz in order to remove the depth degeneracy. Then, the light goes to mirrors thanks to circulators (Cir1 and Cir2). These mirrors reflect the light back through the 50:50 output coupler (Cp2) where the interferometric mixing is achieved. The interferometric signal is then sent into a balanced detection. The two reflected light components will interfere if there path difference is within the coherence length of the swept source (typically 10 mm). Once the spectral interferogram is acquired, its Fourier transform is computed to get the depth profile.
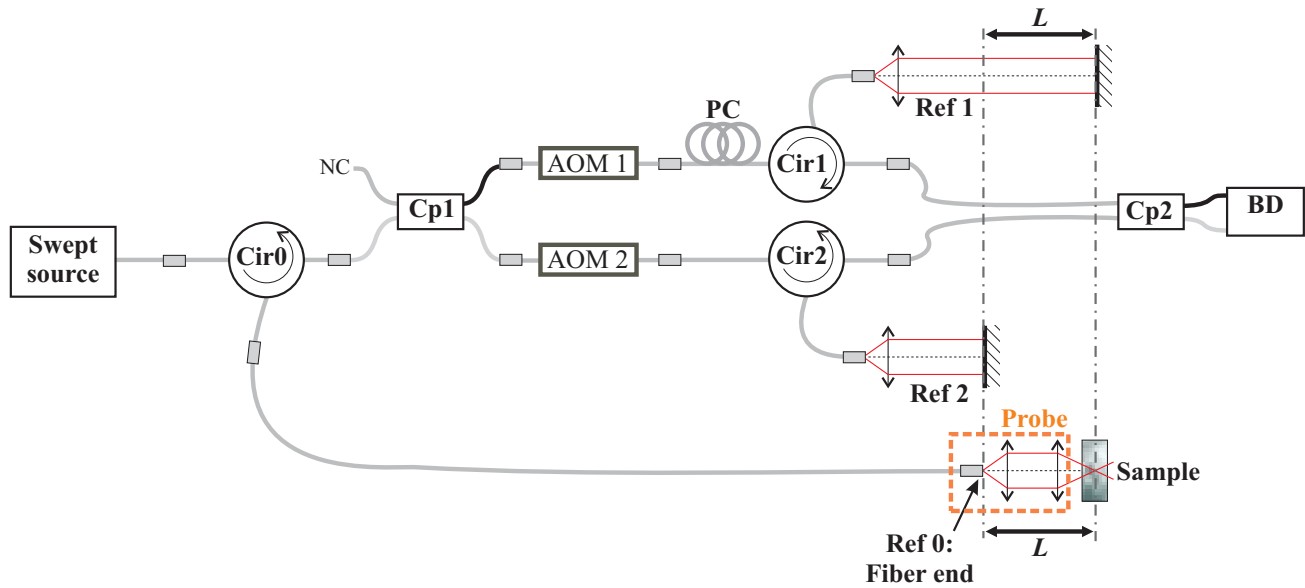

Figure 1. Common path SS-OCT setup with artifact removal. Cp1 and Cp2: couplers, AOM1 and AOM2: Acousto-Optic Modulators, PC: Polarization Controller, Cir0, Cir1 and Cir2: Circulators, BD: Balanced Detection.

The reference interferometer implements a path difference between two fixed mirrors of its two arms. This difference path length is the same as the distance between the fiber tip and the sample surface. Thereby, the reflection from the fiber tip and reflection from the sample surface are traveling the same optical path length. When they are mixed in the output coupler, interferences are observed.

A common-path configuration cumulates several advantages. First, the fiber tip reflection from the sensing probe is used as a position reference. It makes absolute accuracy measurements easier to implement. The optical length fluctuations induced by optical fibers temperature variations can be compensated. Thereby, the knowledge of the absolute position of a surface reflection depends mainly on the accuracy of the mechanical probe actuator. Second, the interferometer can be packaged in a single box and a single optical fiber needs to get out to be connected to the sensing probe. The probe connection can be switched easily, manually or using a remote controlled optical switch, without having to match fiber length as required when using a more "traditional" configuration. A reflection from the tip of the probe, 4 % of the incident power, is obtained by selecting a straight cut fiber (0 deg.) instead of the usual angled-polished fiber (8 deg.) which practically eliminates the

power reflected back in the fiber. Such a feature has been proposed by Waters et al.[22] We observed that 4 % is often a large value compared to the light that is collected back from the sample surface. Using a smaller angle cut, 2 degrees for example, or an anti-reflection coating over a straight cut would attenuate the reflection to a smaller fraction of the incoming signal, between 0.25 % and 1 %, and would improve the signal-to-noise ratio. That feature was implemented in our laboratory several years ago. Recently, Sharma et Al.[23] have quantified with a time-domain OCT setup the signal to noise ratio improvement that results when the tip reflectivity is reduced.

At last, it must be kept in mind that in SS-OCT, the fiber tip reflection should not be too strong otherwise the signal seen by the detector at the output of the interferometer will be saturated and will pollute the A-scans.

3. THEORETICAL BACKGROUND

Let be E the field at the output of the interferometer. It can be written as:

$$E = E_{F1} + E_{F2} + E_{S1} + E_{S2} \tag{1}$$

where E_{F1} and E_{F2} comes from the fiber tip reflection through the Ref1 and Ref2 respectively, E_{S1} and E_{S2} comes from the sample reflection through the Ref1 and Ref2.

Thus, what sees the detector gives:

$$
\begin{aligned}
|E|^2 &= (E_{F1} + E_{F2} + E_{S1} + E_{S2}) \cdot (E_{F1}^* + E_{F2}^* + E_{S1}^* + E_{S2}^*) \\
&= E_{F1}E_{F1}^* + E_{F2}E_{F2}^* + E_{S1}E_{S1}^* + E_{S2}E_{S2}^* \\
&\quad + (E_{F1}E_{F2}^* + E_{F1}^*E_{F2}) + (E_{F1}E_{S1}^* + E_{F1}^*E_{S1}) + (E_{F1}E_{S2}^* + E_{F1}^*E_{S2}) \\
&\quad + (E_{F2}E_{S1}^* + E_{F2}^*E_{S1}) + (E_{F2}E_{S2}^* + E_{F2}^*E_{S2}) + (E_{S1}E_{S2}^* + E_{S1}^*E_{S2})
\end{aligned} \tag{2}
$$

After rearrangement, taking into account that $I_{Xn} = |E_{Xn}|^2$ where X stands for F or S and $n = [1, 2]$, it comes:

$$
\begin{aligned}
|E|^2 &= I_{F1} + I_{F2} + I_{S1} + I_{S2} \\
&\quad + 2\sqrt{I_{F1}I_{S2}} \cdot \cos\left[\frac{2\pi}{c}\nu\Big(L_1 - (L_2 + L)\Big)\right] \\
&\quad + 2\sqrt{I_{F2}I_{S1}} \cdot \cos\left[\frac{2\pi}{c}\nu\Big(L_2 - (L_1 + L)\Big)\right] \\
&\quad + 2\sqrt{I_{F1}I_{F2}} \cdot \cos\left[\frac{2\pi}{c}\nu(L_1 - L_2)\right] + 2\sqrt{I_{S1}I_{S2}} \cdot \cos\left[\frac{2\pi}{c}\nu\Big((L_1 + L) - (L_2 + L)\Big)\right] \\
&\quad + 2\sqrt{I_{F1}I_{S1}} \cdot \cos\left[\frac{2\pi}{c}\nu L\right] + 2\sqrt{I_{F2}I_{S2}} \cdot \cos\left[\frac{2\pi}{c}\nu L\right]
\end{aligned} \tag{3}
$$

In this equation, we see in the first row the four DC components. The four last rows could potentially contribute to the interference fringes, provided that the optical path delay in each term is lower than the coherence length (L_c) of the source. Nevertheless, what is interesting is the fringes achieved between the end of the fiber and the sample. Therefore, let's have $L_1 - (L_2 + L) < L_c$ and fringes will appear in the second row. As we can place the sample to have $L \gg L_c$, it can be inferred that $L_1 - L_2 \gg L_c$ and $L_2 - (L_1 + L) \gg L_c$. As a consequence, no fringes will theoretically appear from the three last rows. At last, it must be kept in mind that the Fourier transform of $|E|^2$ is computed to get the A-scan.

4. SYSTEM CHARACTERIZATION AND COMPARISON

4.1 Envelope Stability

To evaluate the envelope stability of the different setup configurations, strong perturbations obtained by twisting the sample arm fiber were introduced. In that case, the sample is a 150 μm thick glass slide and 50 averaged A-scans were measured at the same location of the sample. The results are plotted in Fig. 2.
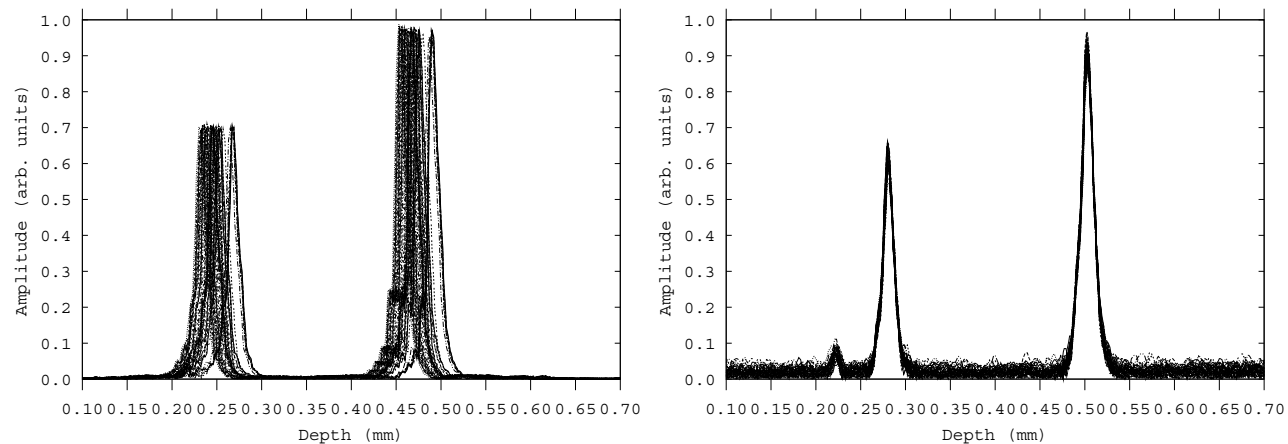
Figure 2. Comparison of the envelope stability of the traditional configuration (left) versus the common path configuration (right). In each case, there are 50 curves corresponding each to an average of 50 A-scans.

Table 1. Position of the different reflectors as a function of the setup used

	Traditional		Common Path	
Position	Mean (mm)	Stand. Dev. (mm)	Mean (mm)	Stand. Dev. (mm)
Reflector 1	0.244	0.012	0.2806	0.0002
Reflector 2	0.466	0.012	0.5028	0.0003

Table 1 summarizes the main data concerning the envelope stability of these setups. In the traditional configuration, the maximum shift between 2 A-scans is close to 40 μm whereas it is lower than 2 μm in the common-path configuration.

One can conclude that the common-path configuration is much more stable than the traditional configuration. It means that, this configuration should be privileged when using, for example, handheld probes.

4.2 Point Spread Function

The other characteristic we studied is the sensitivity. To appreciate the sensitivity of each configuration, the point spread function (PSF) was measured for different optical path length. A mirror was used as a sample and an average of 50 A-scans was computed to plot the PSFs. Figure 3 shows the PSFs as a function of the optical delay for each configuration.

The dynamic range of the traditional configuration is greater than 50 dB. The dynamic range is lower in common-path configuration especially when using the AOM common-path configuration. It is partly due to the fact that the interferometric signal is much weaker in common path configuration. Thus, we cannot take advantage of the whole dynamic range of the data acquisition board because of the poor signal-to-noise ratio. Moreover an artifact around -1.2 mm can be seen. It is due to crosstalk between the two acquired channels. We can also note a pass band effect due to an electronic filter put after the balanced detection. These are currently limitations for our actual setup and we are addressing these to improve the efficiency of our common-path implementation.

5. EXAMPLE OF IMAGES

This section presents images obtained with a common-path configuration with and without artifact removal.

5.1 Optical Phantom

First measurements were made on an in-house phantom. Actually, we produce in our institute durable phantoms of various scatterers embedded in room temperature vulcanizing silicones.[24]
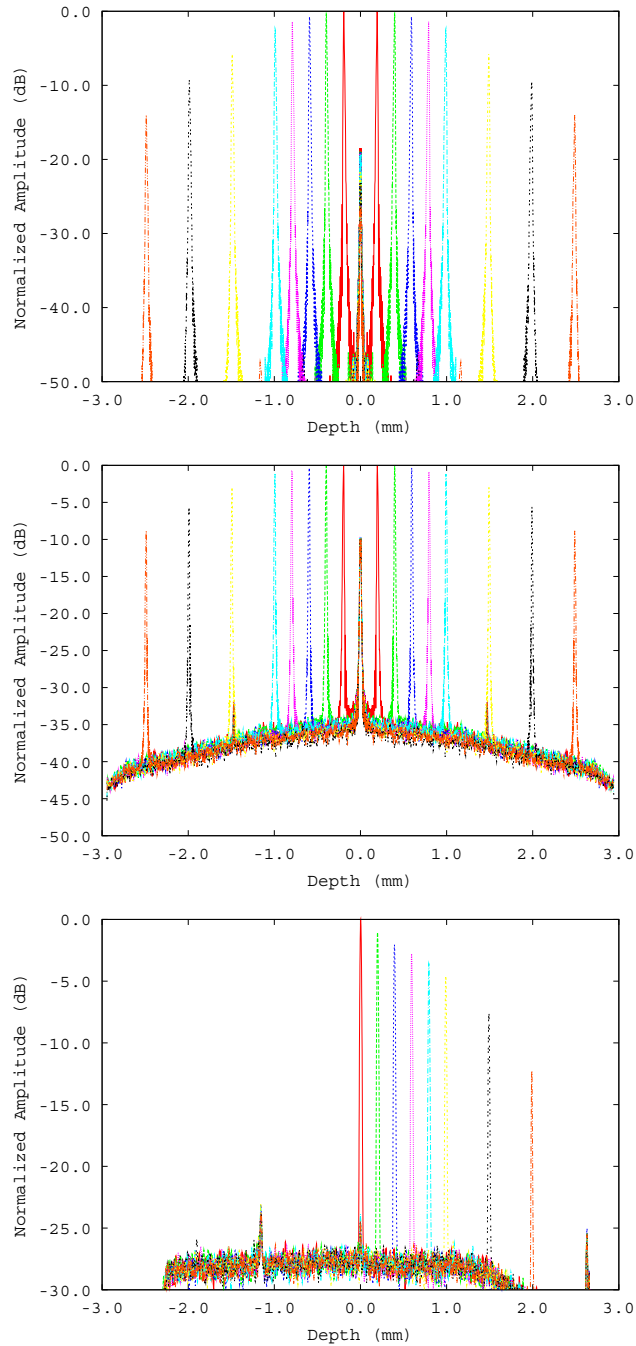
Figure 3. Measured point spread function for different delays. The normalized amplitude is expressed as $20 \cdot \log(\mathcal{F}[I])$ where $\mathcal{F}$ is the Fourier transform and I is measured at the output of the interferometer. Top: traditional configuration, middle: common-path configuration, bottom: common-path configuration with acousto-optic modulators.

Figure 4 shows images of a phantom with alumina micron size powder.
In spite of the low sensitivity, we clearly see the effect of the artifact removal setup. Actually, the scatterers of the phantom appear very well on the corrected image whereas they are all mixed in the non-corrected image.
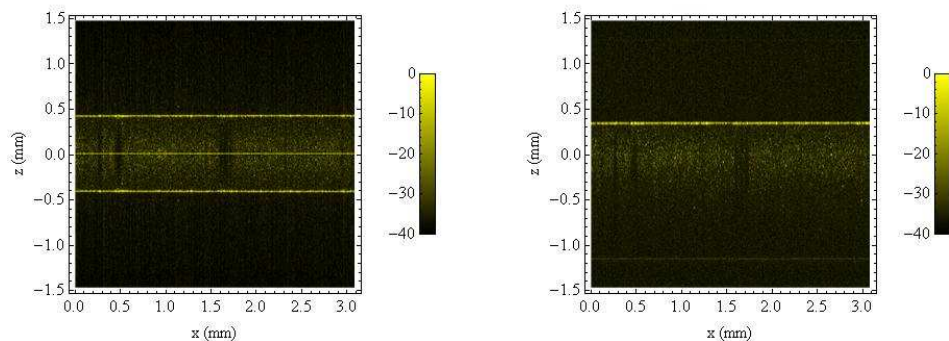
Figure 4. Common path SS-OCT images of an in-house phantom without (left) and with (right) acousto-optic modulators.
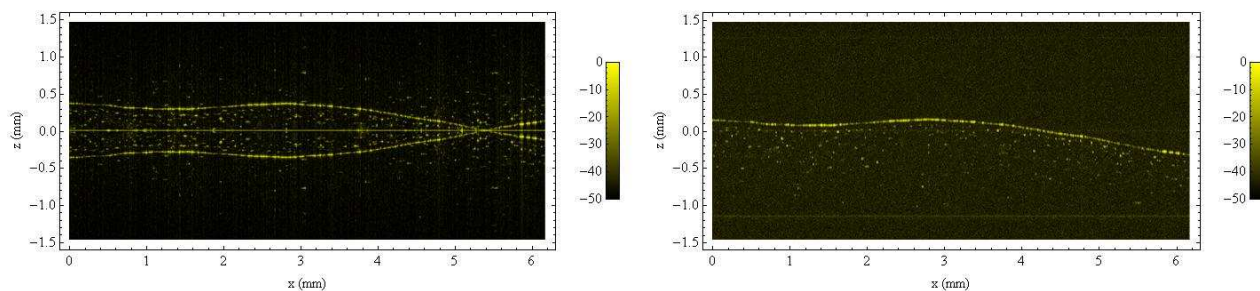
5.2 Onion

An onion was imaged in Fig. 5.

Figure 5. Common path SS-OCT images of an onion without (left) and with (right) acousto-optic modulators.

Once again, the effect of the artifact removal setup is illustrated here. Nevertheless, the low sensitivity of the AOM common-path configuration penalizes the quality of the image.

6. CONCLUSION

In this paper, we have presented a common-path SS-OCT setup with artifact removal. This configuration is useful for application where stability is required. It is also very convenient when handled probes are required. Besides, it enables easy probe exchange without spending time to match the optical path delay between the reference and the sample arms. It makes also possible absolute accuracy measurements. It must be noted that the phase stability is better with a common-path configuration even if these results have not been included in that paper.

At last, the lower sensitivity of the common-path configuration does not lead to image quality as good as with the "traditional" configuration. Work is still in progress in that way to significantly improve the sensitivity of this common-path configuration.

ACKNOWLEDGMENTS

REFERENCES

1. Flournoy, P. A. , "Interferometric optical phase discrimination apparatus," US patent 3319515 (1967).
2. Flournoy, P. A. , McClure, R. W. , and Wyntjes, G. , "White-light interferometric thickness gauge," Applied Optics 11(9), 1907–1915 (1972).
3. Bosselmann, T. and Ulrich, R. , "High-accuracy position-sensing with fiber-coupled white-light interferometers," in *Proceedings of the SPIE* 514, 361–364 (1984).
4. Sorin, W. V. , "Apparatus for measuring the thickness of a moving film utilizing an adjustable numerical aperture lens," US patent 5473432 (1995).
5. Dufour, M. L. , Lamouche, G. , Vergnole, S. , Gauthier, B. , Padioleau, C. , Hewko, M. , Levesque, S. , and Bartulovic, V. , "Surface inspection of hard to reach industrial parts using low-coherence interferometry," in *Photonics North 2006*, Mathieu, P. , ed., 6343, 63 431Z–7 (2006).
6. Vakhtin, A. B. , Kane, D. J. , Wood, W. R. , and Peterson, K. A. , "Common-Path Interferometer for Frequency-Domain Optical Coherence Tomography," Applied Optics 42(34), 6953–6958 (2003).
7. Popp, A. , Wendel, M. , Knels, L. , Knuschke, P. , Mehner, M. , Koch, T. , Boller, D. , Koch, P. , and Koch, E. , "Common-Path Fourier Domain Optical Coherence Tomography of Irradiated Human Skin and Ventilated Isolated Rabbit Lungs," in *Optical Coherence Tomography and Coherence Techniques II,*, Drexler, W. , ed., 5861, paper TuB2 (2005).
8. Tumlinson, A. R. , Barton, J. K. , Povaay, B. , Sattman, H. , Unterhuber, A. , Leitgeb, R. A. , and Drexler, W. , "Endoscope-tip interferometer for ultrahigh resolution frequency domain optical coherence tomography in mouse colon," Optics Express 14(5), 1878–1887 (2006).
9. Feldchtein, F. I. and Gelikonov, G. V. , "Common path frequency domain optical coherence reflectometer and common path frequency domain optical coherence tomography device," US patent App 20070008545 (2007).
10. Bachmann, A. H. , Michaely, R. , Lasser, T. , and Leitgeb, R. A. , "Dual beam heterodyne Fourier domain optical coherence tomography," Optics Express 15(15), 9254–9266 (2007).
11. Zhang, J. , Nelson, J. S. , and Chen, Z. , "Removal of a mirror image and enhancement of the signal-to-noise ratio in Fourier-domain optical coherence tomography using an electro-optic phase modulator," Optics Letters 30(2), 147–149 (2005).
12. Yun, S. H. , Tearney, G. J. , de Boer, J. F. , and Bouma, B. E. , "Removing the depth-degeneracy in optical frequency domain imaging with frequency shifting," Optics Express 12(20), 4822 – 4828 (2004).
13. Davis, A. M. , Choma, M. A. , and Izatt, J. A. , "Heterodyne swept-source optical coherence tomography for complete complex conjugate ambiguity removal," Journal of Biomedical Optics 10(6), 064 005–1 – 064 005–6 (2005).
14. Sarunic, M. V. , Applegate, B. E. , and Izatt, J. A. , "Real-time quadrature projection complex conjugate resolved Fourier domain optical coherence tomography," Optics Letters 31(16), 2426–2428 (2006).
15. Wojtkowski, M. , Kowalczyk, A. , Leitgeb, R. , and Fercher, A. F. , "Full range complex spectral optical coherence tomography technique in eye imaging," Optics Letters 27(16), 1415–1417 (2002).
16. Yasuno, Y. , Makita, S. , Endo, T. , Aoki, G. , Itoh, M. , and Yatagai, T. , "Simultaneous B-M-mode scanning method for real-time full-range Fourier domain optical coherence tomography," Applied Optics 45(8), 1861–1865 (2006).
17. Wang, R. K. , "In vivo full range complex Fourier domain optical coherence tomography," Applied Physics Letters 90(5), 054 103–3 (2007).
18. Baumann, B. , Pircher, M. , Gtzinger, E. , and Hitzenberger, C. K. , "Full range complex spectral domain optical coherence tomography without additional phase shifters," Opt. Express 15(20), 13 375–13 387 (2007).
19. An, L. and Wang, R. K. , "Use of a scanner to modulate spatial interferograms for in vivo full-range Fourier-domain optical coherence tomography," Opt. Lett. 32(23), 3423–3425 (2007).
20. Leitgeb, R. A. , Michaely, R. , Lasser, T. , and Sekhar, S. C. , "Complex ambiguity-free Fourier domain optical coherence tomography through transverse scanning," Opt. Lett. 32(23), 3453–3455 (2007).
21. Vergnole, S. , Lamouche, G. , and Dufour, M. , "Artifact removal in Fourier-domain optical coherence tomography with a piezoelectric fiber stretcher," Opt. Lett. accepted for publication (2007).
22. Waters, J. P. and Fernald, M. R. , "Common optical path interferometric gauge," US patent 4627731 (1986).

23. Sharma, A. , Fried, N. M. , and Kang, J. U. , "All-fiber common-path optical coherence tomography: sensitivity optimization and system analysis," IEEE Journal of Selected Topics in Quantum Electronics 11(4), 799–805 (2005).

24. Bisaillon, C.-E. , Lamouche, G. , Lanthier, M.-M. , Lévesque, D. , Maciejko, R. , and Monchalin, J.-P. , "Deformable and durable optical phantoms with controlled number of scatterers," in *Design and Performance Validation of Phantoms Used in Conjunction with Optical Measurements of Tissue* 6870, Paper 6870–10 (2008).